Chapter 11

Stellar dynamos

ELWOOD: It's 106 miles to Chicago, we've got a full tank of gas, half a pack of cigarettes, it's dark and we're wearing sunglasses.
JAKE: Hit it!

Dan Ackroyd and John Belushi
The Blues Brothers (1980)

The problem —and the beauty— with the Sun is that it overwhelms us with data. Many of the intricacies we have busied ourselves with in the preceding chapter were directly motivated by the detailed observations and magnetic measurements made possible by the sun's astronomical proximity. The sun remains for sure an exemplar, but with other stars observational contraints are much more sparse, and theoretical considerations take on an enlarged role.

So, it's back to basics. What have we learned in the preceding three chapters about dynamo action in electrically conducting fluids? At the most fundamental level, a top-three list could run as follows:

- We learned in chapter 7 that rotation, and especially differential rotation, is one very powerful mechanism allowing to build a large-scale magnetic field;
- We learned in chapter 8 that flows with chaotic trajectories, such as arising from strongly turbulent convection, can act as dynamos;
- We learned in chapter 9 that in turbulent flows, the presence of rotation and stratification can break rotational symmetry and produce a self-amplifying large-scale magnetic field.

So, offhand we are not in too bad a shape with regards to stellar dynamos. Stars certainly are stratified, and certainly rotate. Thermally-driven convection is also present across large-part of the HR diagram, but here we start to encounter complications that restrict the use of the "solar exemplar". Figure 11.1 illustrates, in schematic form, the internal structure of main-sequence stars, more specifically the presence or absence of convection zones. A G-star like the Sun has a thick outer convection zone, spanning the outer 30% in radius in the solar case. As one moves down to less massive stars, the relative thickness of the convective envelope increases until, somewhere in the M spectral range, stars become fully convective. Exactly at what mass the radiative core disappears depends on metallicity, opacities, and so on. Moving instead from the Sun to higher masses, the convective envelope becomes ever thinner, until somewhere around spectral-type A0 it essentially vanishes. However, at around the same spectral type Hydrogen burning switches from the p-p chain to the CNO cycle, for which nuclear reaction rates are much more sensitively dependent on temperature. Core energy release becomes strongly depth-dependent, leading to a steep —and convectively unstable— temperature gradient. This produces a small convective core, which grows in size as one moves up to larger masses. In a

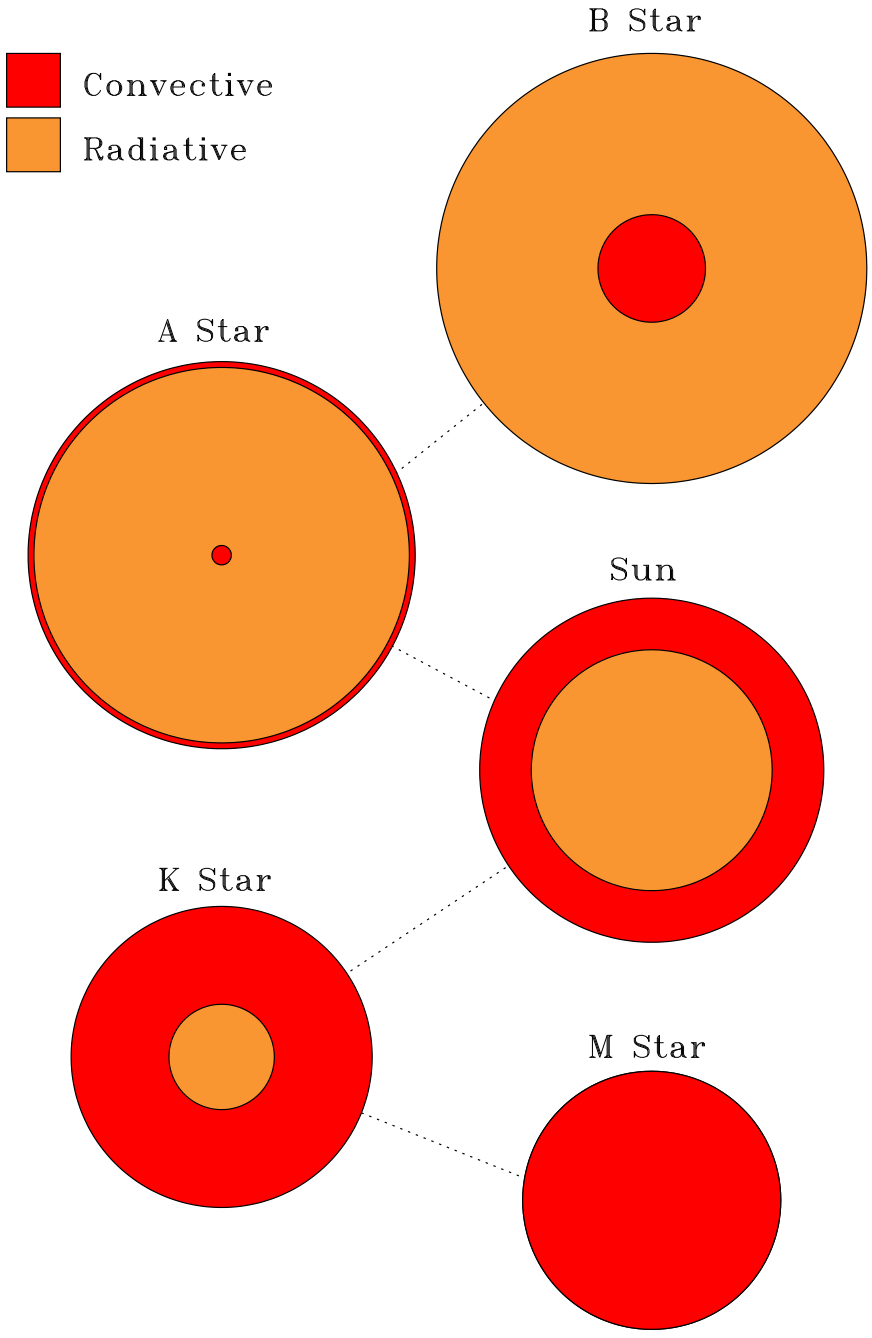

Figure 11.1: Schematic representation of the radiative/convective internal structure of main-sequence stars. The thickness of the outer convection zone for the A-star is here greatly exaggerated; drawn to scale it would be thinner than the black circle delineating the stellar surface on this drawing. Relative stellar sizes are also not to scale.

"typical" B-star of solar metallicity, the convective core spans the inner 25% or so in radius of the star.

From these simple considerations, A-stars immediately stand out as the least likely to support dynamo action, because they lack a convective region of substantial size. This squares well with various lines of observations; in particular, main-sequence A-stars are amongst the most "magnetically quiet" stars in the HR diagram, as far as things like X-Ray emission and flaring is concerned. Indeed, the chemically peculiar Ap stars discussed in chapter 2 do show strong magnetic fields, but even those show no sign of anything even mildly analogous to solar activity. This is why to this day the fossil field hypothesis remains the favored explanatory model for the magnetic field of Ap stars (but do see some of the references in the bibliography for alternative explanations).

Until strong evidence to the contrary is brought to the fore, we are allowed to assume that late-type stars with a thick convective envelopes overlying a radiative core host a solar-type dynamo. This is buttressed by the observation of solar-like cyclic activity in many such stars (as briefly discussed already many, many pages ago in §2.4). We will therefore begin (§11.1) by looking into the way(s) the various types of solar-cycle models considered in the preceding chapter can be "scaled" to other solar-type stars, of varying masses, rotation rates, etc.

With fully convective stars, we encounter potential deviations from a solar-type dynamo mechanism; without a tachocline and radiative core to store and amplify toroidal flux ropes, the Babcock-Leighton mechanism becomes problematic. Mean-field models based on the turbulent α-effect remain viable, but the dynamo behavior becomes dependent on the presence and strength of differential rotation, about which we really don't know very much in stars other than the sun.

Finally, at the other end of the main-sequence mass range, i.e. O and B stars, the presence of a turbulent convective core combined with high rotation (viz. §5.3) makes dynamo action more than likely. As we shall see in §11.2 below, the challenge is actually to bring the magnetic field produced in the core to the surface.

11.1 Late-type stars other than the Sun

Interms of real observations as opposed to models, most of what we know regarding dynamo activity in solar-type stars comes from the Mt Wilson CaH+K survey described already in §2.4. Two important pieces of information can be extracted from these data, as constraints on dynamo models. The first is the overall level of CaH+K emission, which is taken as a measure of overall photospheric magnetic field strength, consistent with what one observes on the sun at various phases of its activity cycle. The second is of course the cycle period, for stars in which a cycle can be detected (see Fig. 2.8). Figures 11.2 and 11.3 illustrate observed trends in these two quantities as a function of the cycle period. From the point of view of dynamo theory and modelling, the following points are noteworthy:

1. Magnetic activity increases with increasing rotation rate (decreasing $P_{\rm rot}$).
2. Cycle period decreases with decreasing rotation rate.

At a given spectral type the relationship between cycle period and rotation rate is well represented by a power-law of the form $P_{\rm cyc} \propto P_{\rm rot}^n$, with $n = 1.25 \pm 0.5$, but data for all spectral type can be brought to a common power law index by using the ratio of the rotation rate to the convective turnover time; recall from the discussion of the preceding chapter that the latter ratio is supposed to measure the efficiency of the Coriolis force in breaking the mirror-symmetry of convective turbulence, and thus producing a non-zero α-effect. You will recall also that the larger the dynamo number, the more magnetic energy mean-field models can produce (viz. Fig. 10.5). So, in a rough qualitative sense, it sort of fits our (naive) expectations.

In practice, we are facing a number of difficulties in extrapolating our solar dynamo models to stars other than the sun, with convection zones of greater or lesser depths, and a range of rotation rates. At the very least we need to be able to specify:

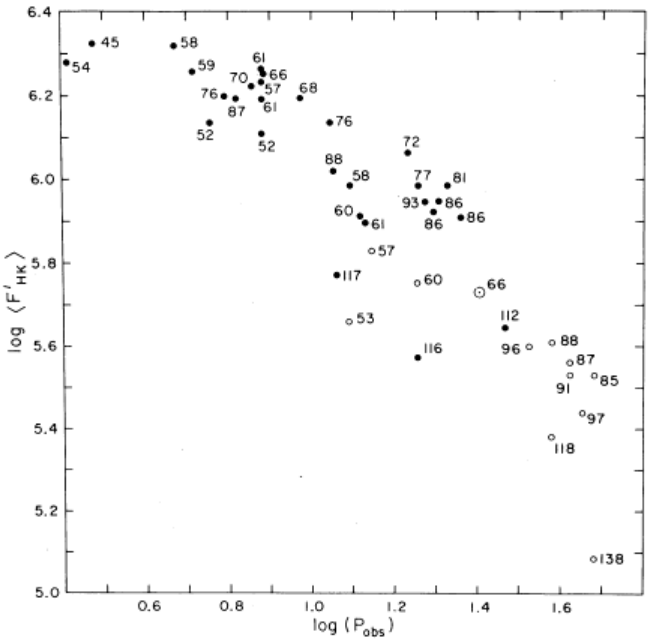

Figure 11.2: Chromospheric activity, taken as an indicator of stellar magnetic field strength, versus rotation period, in a sample of solar-type stars of various surface temperature (as individually labeled in terms of $100 \times (B - V)$). Figure taken from Noyes *et al.* (1984), *The Astrophysical Journal*, **279**, 763 [Fig. 6].

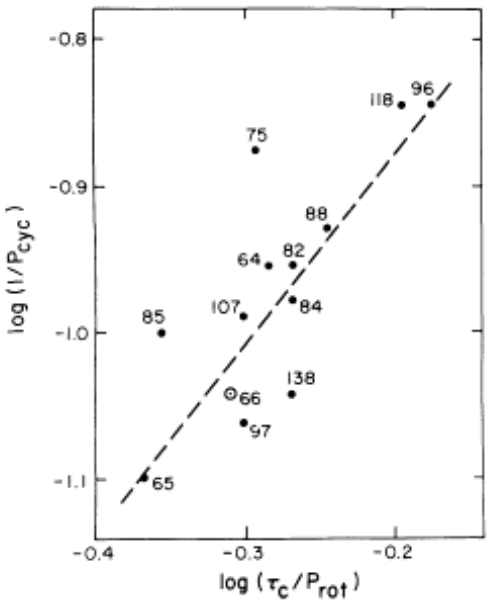

Figure 11.3: Relationship between Cycle period ($P_{\rm cyc}$) and the ratio of convective turnover time (τ_c) to the rotation period ($P_{\rm rot}$) for the subsample of the stars in the above Figure for which cycle periods can be reliably determined. Figure taken from Noyes *et al.* (1984), *The Astrophysical Journal*, **287**, 769 [Fig. 2].

1. How the form and magnitude of differential rotation and meridional circulation change with rotation rate and luminosity, the latter determining the magnitude of convective velocities, and thus the magnitude of the turbulent Reynolds stresses powering the large-scale flows important for dynamo action;

2. How the α-effect and turbulent diffusivities vary in stars with rotation rate and convection zone properties;

3. How the process of sunspot formation (Babcock-Leighton models) vary with varying convection zone depth, rotation, etc.

Even then, the discussion of the preceding chapter should have made it clear that even in the sun, we don't really know for sure what is the mechanism responsible for the regeneration of the poloidal magnetic component. How then can we hope to go about modelling stellar dynamos with anything resembling confidence?

The problem can be turned around, in that stellar cycle observations can perhaps be used to distinguish between different classes of dynamo models! The possibility hinges on the distinct dependency of the cycle period on model parameters in various models. For the α-quenched mean-field solutions discussed in §10.2.3, the (dimensionless) cycle period is, to a first approximation, independent on the dynamo numbers (see Fig. 10.3B), so that the physical period scales primarily as

$$P_{\rm cyc} \propto \eta^{-1} \ , \qquad [\alpha-\text{quenched } \alpha\Omega \text{ model}] \tag{11.1}$$

where η is the assumed turbulent diffusivity. On the other hand, in Babcock-Leighton dynamo models the cycle period is found to be controlled primarily by the turnover time of the meridional flow cell. For the specific "solar" model described in §10.3, the cycle period is found to vary as:

$$P_{\rm cyc} \propto u_0^{-0.89} s_0^{-0.13} \eta^{-0.22} \ , \qquad [\text{Babcock} - \text{Leighton}] \tag{11.2}$$

where u_0 is the surface meridional flow speed (see Fig. 10.2), and s_0 is the parameter measuring the magnitude of the Babcock-Leighton source term in eq. (10.46)[1]. Unfortunately, using this relationship in conjunction with observed stellar cycle data requires one to specify how the meridional flow speed varies with rotation, which currently remains highly uncertain on the theoretical and simulation fronts. But this is a very promising avenue.

What happens when main-sequence stars become cool enough to be fully convective is yet another possible discriminant. Is it possible to produce sunspots —and thus a Babcock-Leighton poloidal regeneration mechanism— if there is no stably stratified tachocline to form and store toroidal flux ropes? We just don't know at this point, but observationally no obvious discontinuity is observed in X-Ray CaK emission as one moves into spectral types M where stars become fully convective.

There is a lot of work to be done in this area... and perhaps some of you will contribute as part of your end-o-semester project!

11.2 Early-type stars

In this final section, we turn to dynamo action in massive stars[2], which will also be an excuse to examine dynamo action in mean-field models of the α^2 and $\alpha^2\Omega$ varieties. we consider a set of representative mean-field dynamo calculations pertaining to the convective core of a $9M_\odot$ ZAMS stellar model, with luminosity $L = 3767 L_\odot$, effective temperature $T_{\rm eff} = 23,600\,{\rm K}$, and

[1]Note however that the above relation was calibrated in a relatively narrow range of parameters: $2 \leq u_0 \leq 30\,{\rm m\ s^{-1}}$, $0.03 \leq s_0 \leq 1\,{\rm m\ s^{-1}}$, $2 \times 10^6 \leq \eta \leq 5 \times 10^7\,{\rm m^2 s^{-1}}$; see the paper by Dikpati & Charbonneau (1999) cited in the bibliography for more details.

[2]The set of dynamo solutions presented here are all taken directly from the Charbonneau & MacGregor (2001) paper cited in the bibliography.

radius $R = 3.678 R_\odot$ (spectral type B2). The radius of the convective core (r_c) in this model is at $r_c = 0.232R$. Within the core, thermally-driven turbulent fluid motions are assumed to give rise to an α-effect and turbulent diffusivity, which both vanish for $r \gtrsim r_c$ (under the assumption that the radiative envelope is turbulence free). In the spirit of the other dynamo models discussed in this chapter, we consider kinematic dynamos with parametric profiles for α and η:

$$\alpha(r,\theta) = \frac{1}{2}\left[1 + \mathrm{erf}\left(\frac{r-r_c}{w}\right)\right]\mathrm{erf}\left(\frac{2r}{w}\right)\cos(\theta) \ , \tag{11.3}$$

$$\eta(r) = \eta_e + \frac{\eta_c - \eta_e}{2}\left[1 - \mathrm{erf}\left(\frac{r-r_c}{w}\right)\right] \ , \tag{11.4}$$

where $\mathrm{erf}(x)$ is once again the error function. Equations (11.3) represent "minimal" assumptions on the spatial dependency of the α-effect: it changes sign across the equator ($\theta = \pi/2$), vanishes at $r = 0$, rises to a maximum value within the convective core, and falls again to zero for $r \gtrsim r_c$, the transition occurring across a spherical layer of thickness $\sim 2w$. we consider models with both positive and negative α-effect.

Various lines of argument related to the rotational evolution of early-type stars suggest that significant differential rotation may exist between the convective core and overlying radiative envelope. In what follows we restrict ourselves to the (simple) case of a convective core and radiative envelope both rotating rigidly but at different rates Ω_c, Ω_e, joined smoothly across a thin spherical shear layer coinciding with the core-envelope interface at $r = r_c$:

$$\Omega(r,\theta) = \Omega_c + \frac{\Omega_e - \Omega_c}{2}\left[1 + \mathrm{erf}\left(\frac{r-r_c}{w}\right)\right] \ . \tag{11.5}$$

The rotation increases inward, i.e., $\Omega_c > \Omega_e$, leading to a negative radial shear in the vicinity of the core-envelope interface[3]. The parameter w used to specify the thickness of the shear layer is the same as that used to specify the width of the transition region for the turbulent diffusivity and α-effect. We are now solving the dynamo equations in their $\alpha^2\Omega$ incarcation, as given by eqs. (9.73)–(9.74), with $\mathrm{R}_m = 0$ but with all other terms present. All dynamo solutions discussed below are obtained as eigenvalue problems, as in §10.2.2. Remember that such linear solutions leave the absolute scale of the magnetic field unspecified.

An interesting physical quantity accessible from linear models is the ratio of the surface field field strength to the field strength in the dynamo region, here the convective core. In what follows we use towards this purpose the ratio (Σ) of the r.m.s. surface poloidal field to the r.m.s. poloidal field at the core-envelope interface r_c:

$$\Sigma = \left(\frac{R^2 \int |\nabla \times A|^2_{r=R} \sin\theta \mathrm{d}\theta}{r_c^2 \int |\nabla \times A|^2_{r=r_c} \sin\theta \mathrm{d}\theta}\right)^{1/2} \ . \tag{11.6}$$

In practice, the finite numerical accuracy at which the eigenfunctions are computed leads to a lower bound on meaningful values of Σ, here at about 10^{-8}. Another useful quantity produced in linear solutions is the toroidal-to-poloidal field strength ratio (Θ), which can be defined as

$$\Theta = \frac{\int B^2 \mathrm{d}V}{\int (\nabla \times (A\hat{\mathbf{e}}_\phi))^2 \mathrm{d}V \ .} \tag{11.7}$$

11.2.1 α^2 dynamos

We first consider solutions where magnetic field generation occurs exclusively through the agency of the α-effect, i.e., α^2 dynamo models, in the terminology introduced in §9.4.3. Figure

[3]Negative radial shear profiles are the only ones considered here, since steep positive radial shears are in all likelihood hydrodynamically unstable.

11.4 shows a series of typical linear α^2 solution with increasing diffusivity contrasts between the core and envelope. The value of C_α for the solutions on panels B, C and D were adjusted to yield solutions with growth rates similar to that of the constant-η solution in A, so that the four eigenfunctions are in some sense comparable.

The constant-η solution transits from decaying ($\sigma < 0$) to growing ($\sigma > 0$) at $C_\alpha \simeq -32.8$, and the growth rate keeps increasing as $|C_\alpha|$ is further increased. The solution plotted on Fig. 11.4A is computed for $C_\alpha = -34.5$, and is supercritical ($\sigma = 10.82\tau^{-1}$). A solution with $C_\alpha = +34.5$ has an identical growth rate and eigenfunction, but shows an opposite relative polarity between the poloidal and toroidal components. For $\eta_e/\eta_c \lesssim 0.1$, the symmetric modes now have slightly larger growth rate ($\sigma = 11.0$, 11.8, and $12.5\,\tau^{-1}$ for $\eta_e/\eta_c = 0.1$, 0.01, and 0.001, respectively). Nonetheless, to facilitate comparison with the constant diffusivity solution of part A, the antisymmetric modes are plotted on Figure 11.4B–D. Defining parameters for all solutions plotted on Fig. 11.4 are listed in the top part of Table 11.1 below.

Linear mean-field dynamo of the α^2 type with a time-independent scalar functional $\alpha(r)$ always produce *steady* magnetic fields, i.e., the solution eigenvalue is purely real ($\omega = 0$ in eq. (10.28)). The solution plotted on Figure 11.4A is dipole-like (i.e., antisymmetric), and is the fastest growing solution for our model with constant η, at the adopted value for C_α. The next fastest growing mode is symmetric with respect to the equatorial plane, and has a growth rate only slightly smaller, $\sigma = 10.79\,\tau^{-1}$. This situation is typical of α^2 dynamo solutions using a scalar α-effect[4]. Note that $\sigma = 10$ in dimensionless units amounts to an e-folding time of about 20 yr in dimensional units, leaving no doubt that ample time is available to amplify a weak seed magnetic field in the core of a massive star.

Table 11.1
Parameters and eigenvalues for various α^2 and $\alpha^2\Omega$ solutions

Type	Parity	C_α	C_Ω	η_e/η_c	w/R	σ	ω	Σ	Θ
α^2	A	-34.5	0	1	0.1	10.8	0	1.2×10^{-2}	1.074
α^2	A	-23.0	0	0.1	0.1	8.96	0	2.7×10^{-4}	1.276
α^2	A	-21.0	0	0.01	0.1	9.91	0	$< 10^{-8}$	1.317
α^2	A	-21.0	0	0.001	0.1	10.58	0	$< 10^{-8}$	1.318
$\alpha^2\Omega$	A	-21.0	2000	0.01	0.1	14.6	175	$< 10^{-8}$	3.21
$\alpha^2\Omega$	S	-21.0	2000	0.01	0.1	21.8	186	$< 10^{-8}$	3.21
$\alpha^2\Omega$	A	$+21.0$	2000	0.01	0.1	21.2	184	$< 10^{-8}$	4.27
$\alpha^2\Omega$	S	$+21.0$	2000	0.01	0.1	14.0	172	$< 10^{-8}$	5.32
$\alpha^2\Omega$	S	-24.0	2000	0.01	0.05	19.9	287	$< 10^{-8}$	3.10
$\alpha^2\Omega$	S	-35.0	2000	0.01	0.025	17.7	494	$< 10^{-8}$	2.52

The most significant consequence of a η_e/η_c being smaller than one is perhaps the "trapping" of the magnetic field in the lower part of the radiative envelope, a direct consequence of the difficulty experienced by an external magnetic field to diffusively penetrate a good electrical conductor. This is clearly evident from Table 11.1, in the rapid decrease of the surface-to-core field ratio Σ (see eq. (11.6)) with decreasing diffusivity ratio η_e/η_c. This is long-recognized property of stellar core dynamos, and represents a rather formidable obstacle to be bypassed if the magnetic fields generated by dynamo action in the convective core are to become observable at the stellar surface. As discussed in Schüssler & Pähler, the situation is even worse than Table 11.1 may suggest. In a time-dependent situation, the time needed for the magnetic field to resistively diffuse to the surface can become larger than the star's main-sequence lifetime, for masses in excess of about $5\,M_\odot$.

[4]The α^2 form of the mean-field dynamo equations also admits growing solutions than are non-axisymmetric even though the α-effect profile exhibits axisymmetry with respect to the rotation axis. Growth rates for non-axisymmetric modes are often comparable to those of their axisymmetric counterparts For simplicity, we restrict ourselves here to axisymmetric modes. We note nonetheless that, motivated largely by the challenge posed by planetary magnetic fields, α^2 models can and have been constructed where non-axisymmetric modes are the fastest growing, and dominate in the moderately supercritical nonlinear regime.

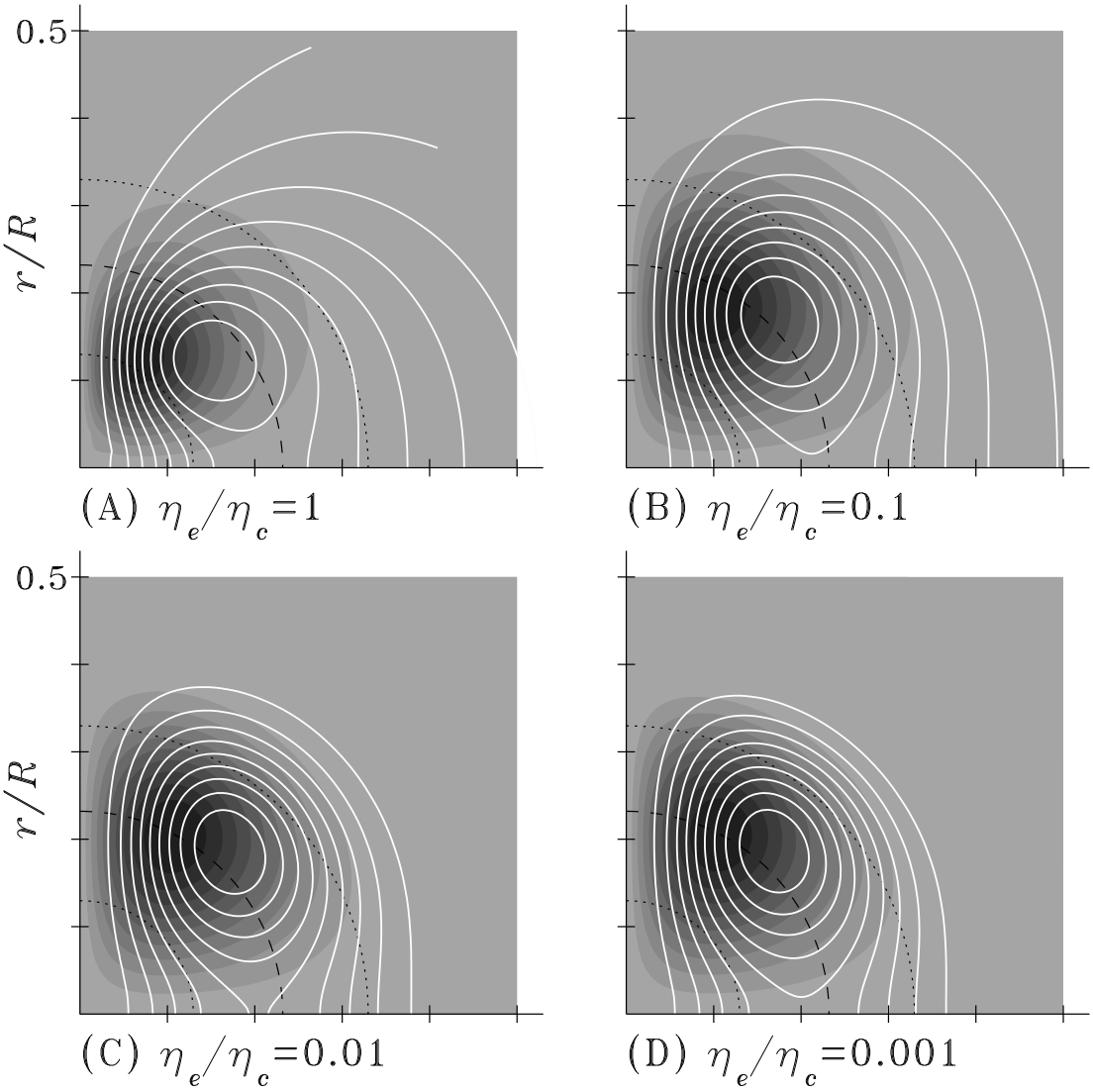

Figure 11.4: Four antisymmetric steady α^2 dynamo solutions, computed using varying magnetic diffusivity ratios between the core and envelope. The solutions are plotted in a meridional quadrant, with the symmetry axis coinciding with the left quadrant boundary. Poloidal field-lines are plotted superimposed on a gray scale representation for the toroidal field (light to dark is weaker to stronger field). The dashed line marks the core-envelope interface depth r_c, and the two dotted lines indicates the depths $r_c \pm w$ corresponding to the width of the transition layer between core and envelope. Note how the solutions with $\eta_e/\eta_c \lesssim 10^{-2}$ have their toroidal field peaking across the core-envelope interface. This behavior is generic and materializes for smaller values of w and r_c, and for symmetric (i.e., quadrupolar-like) solutions. Parameters for these solutions are listed in Table 11.1.

Less striking but equally important in what follows is the fact that in solutions with $\eta_e/\eta_c < 1$, the locus of peak dynamo action —as measured by the peak in toroidal field strength— moves out to the core-envelope boundary. Note on Fig. 11.4 how, for $\eta_e/\eta_c \lesssim 0.01$, toroidal fields are present out to $r \simeq r_c + w$. This is a direct consequence of the α/η ratio remaining equal to unity over a significant radial distance outside of the core, as per eqs. (11.3)—(11.4). As η_e/η_c decreases, the magnetic field is increasingly trapped in the interior, yet is increasingly concentrated near the core-envelope interface. This behavior is robust, in that it also materializes in solutions computed using different parameter values.

Mean-field dynamo models of the α^2 variety typically generate magnetic fields that have poloidal and toroidal components of comparable strengths. Indeed we find here that the toroidal-to-poloidal ratio defined in eq. (11.7) are of order unity and vary very slightly with η_e/η_c (see Table 11.1).

11.2.2 $\alpha^2\Omega$ and $\alpha\Omega$ dynamos

Perhaps the most significant difference between $\alpha^2\Omega$ solutions and the α^2 solutions considered previously is the fact that while the latter are spatially steady (in the sense that $\omega = 0$), the former usually yield oscillatory solutions, with solution eigenvalues occurring in complex conjugate pairs $\sigma \pm i\omega$.

Figure 11.5 illustrates a half-cycle of a representative $\alpha^2\Omega$ solution. This symmetric solution has $C_\alpha = -21$, $C_\Omega = 2000$, $w/R = 0.1$, $\eta_e/\eta_c = 10^{-2}$, and is characterized by a growth rate $\sigma = 21.8\,\tau^{-1}$ and frequency $\omega = 186\,\tau^{-1}$. For $\eta_c = 10^{13}\,\mathrm{cm^2\,s^{-1}}$, this corresponds to a dynamo period of about 7 yr, quite short compared to any other relevant timescales. The magnetic field distribution is shown at five distinct phases, at constant intervals of $\Delta\varphi = \pi/4$, in a format identical to that of Fig. 11.4 for each panel (note in particular that the eigenmodes are again plotted only in the inner half of the star). At a given phase the solutions bear some resemblance to the α^2 solutions of Fig. 11.4C, in that the magnetic field is again trapped in the interior. As before, the toroidal field is concentrated near the core-envelope interface, and in fact here peaks slightly outside $r = r_c$ (dashed circular arc).

As with the α^2 solutions considered previously, the growth rate of the $\alpha^2\Omega$ solution increases with increasing values of either or both the dynamo numbers C_α and C_Ω. The dynamo frequency ω also increases with C_α and C_Ω. In the $\alpha\Omega$ limit, where the α-effect makes a vanishing contribution to the RHS of eq. (9.74), the eigenvalue is completely determined by the value of the product $C_\alpha C_\Omega$, but this property does not hold in general for $\alpha^2\Omega$ models.

Examination of Figure 11.5 soon reveals that the magnetic field distribution migrates steadily poleward in the course of the half-cycle shown on Figure 3, with the solutions at $\varphi/\pi = 1$ being a mirror image of that at $\varphi/\pi = 0$, i.e., the magnetic polarity has undergone a polarity reversal after half an oscillation cycle. This is the "dynamo wave" we already encountered previously, and indeed the poleward propagation observed here is what one would expect from a negative radial shear acting in conjunction with a negative α-effect (cf. §9.3). [5]. Note that the toroidal field gains in strength as the dynamo wave proceeds from low to mid-latitudes, peaking at about 60° and falling thereafter as the wave experiences enhanced dissipation upon converging toward the symmetry axis.

A solution with $C_\alpha = +21$ but otherwise identical to that shown on Fig. 11.5 has growth rate and frequency that are comparable to, but not identical to the $C_\alpha = -21$ solution (see Table 11.1). The difference is due to spherical geometry; a poleward-propagating dynamo wave suffers greater diffusive decay as it converges towards the symmetry axis, than an equatorward propagating wave does converging towards the equatorial plane, where the symmetry imposed via the boundary condition also affects the dissipation. Solutions with thinner transition layers require a larger value of $|C_\alpha|$ to maintain comparable growth rates, and are thus characterized

[5] Parker's original dynamo wave solutions were obtained in Cartesian geometry, and in the so-called $\alpha\Omega$ limit, in which the α-effect is omitted on the RHS of the toroidal component of the dynamo equation. Similar dynamo wave solutions are also readily found in the more general $\alpha^2\Omega$ case; see for example the Choudhuri (1990) paper cited in the bibliography.

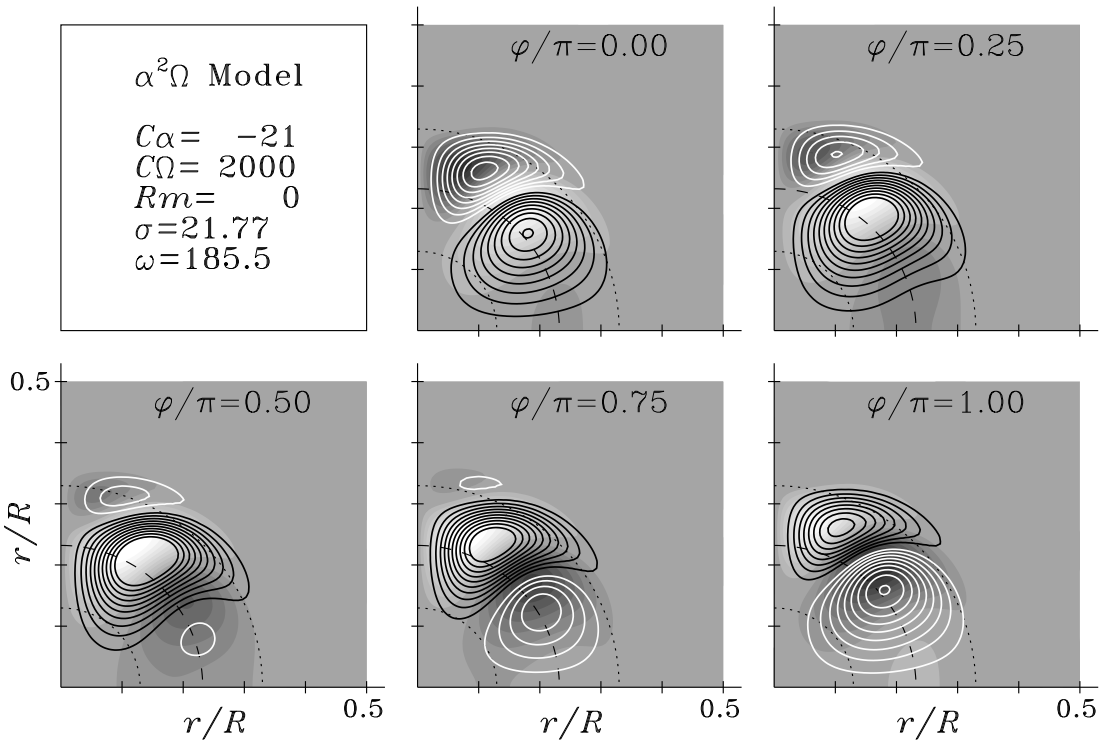

Figure 11.5: A representative $\alpha^2\Omega$ solution. As this is an oscillatory solution, the eigenfunction is plotted at five equally spaced phase intervals ($\Delta\varphi = \pi/4$), covering half an oscillation cycle. The format in each panel is similar to Fig. 11.4. White (black) lines indicate fieldlines oriented in a clockwise (counterclockwise) direction. Note the wave-like propagation of the magnetic field from low to high latitudes. Parameter values are listed in Table 11.1.

by higher oscillation frequencies. Table 11.1 lists solution parameters and characteristics for a few representative such solutions.

Not surprisingly, in $\alpha^2\Omega$ models the availability of an additional energy source in the toroidal component of the dynamo equations leads to solutions where the toroidal field strength in general exceeds that of the poloidal field. For the solution plotted on Fig. 11.5, the toroidal-to-poloidal field ratio (see eq. (11.7)) reaches a value $\Theta \simeq 3$. Further increases of C_Ω lead to increasing Θ (e.g., $\Theta \simeq 3.4$ and 4.3 at $C_\Omega = 5000$ and 10^4), until in the $\alpha\Omega$ limit Θ scales roughly as C_Ω/C_α. For a given diffusivity ratio η_e/η_c, oscillatory $\alpha^2\Omega$ solutions have a smaller surface-to-core field strength ratio Σ than α^2 models, a direct consequence of the oscillatory nature of the field, which restricts the radial extent of the eigenfunction above the core-envelope interface to a distance comparable to the electromagnetic skin depth, which is very much smaller than the stellar radius for $\eta_e/\eta_c \ll 1$.

The markedly different spatial distributions and temporal behavior of α^2 and $\alpha^2\Omega$ eigenmodes naturally leads one to suspect that both dynamo modes should have some difficulty operating simultaneously. That this is indeed the case can be seen in Figure 11.6, showing isocontours of the linear growth rate σ in the $[C_\Omega, C_\alpha]$ plane, for antisymmetric negative-C_α solutions. Dynamo solutions ($\sigma > 0$) are located below the thick contour, and the thick dashed line delineates the regions where steady ($\omega = 0$, α^2-like) and oscillatory ($\omega \neq 0$, $\alpha^2\Omega$-like) solutions are found. At a fixed value of C_α, introducing differential rotation first leads to a *decrease* of the growth rate, reflecting the perturbative influence of differential rotation on the basic α^2 mode. Once C_Ω exceeds a certain (C_α-dependent) threshold at about $C_\Omega \simeq 300$, the dynamo becomes $\alpha^2\Omega$-like ($\omega \neq 0$). However, growth rates comparable to that of the pure α^2 mode ($C_\Omega = 0$) materialize only for much larger values of C_Ω. Much the same behavior is seen

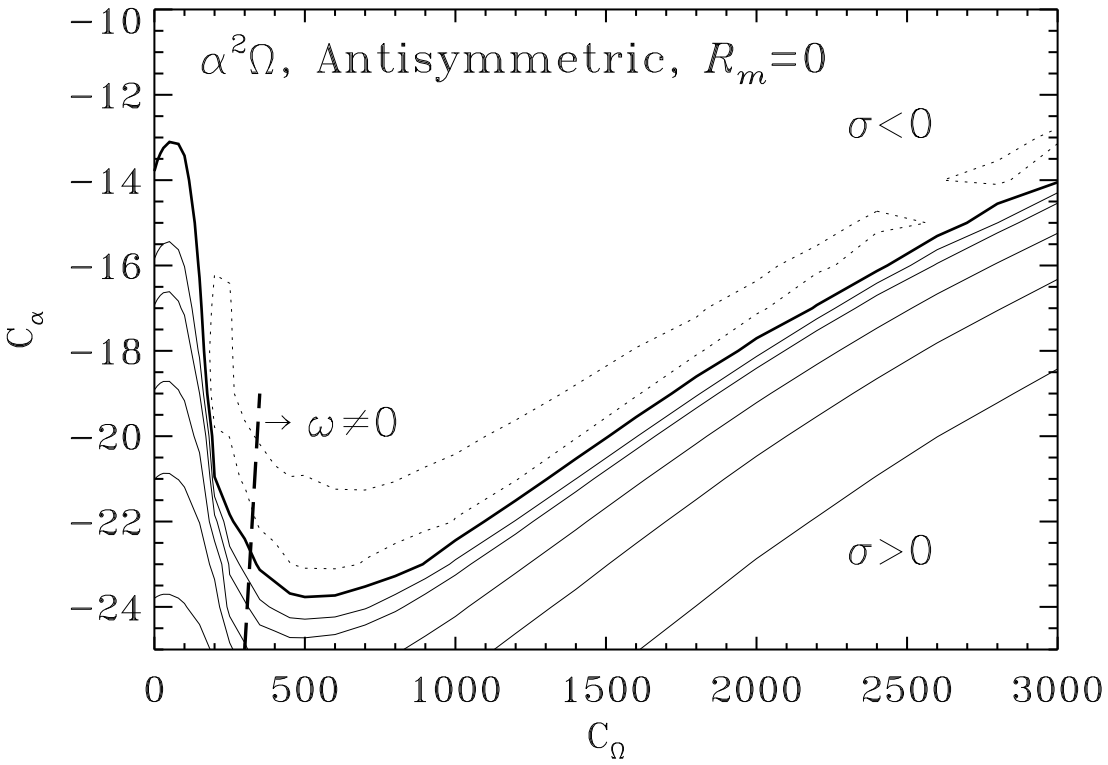

Figure 11.6: Isocontours of the $\alpha^2\Omega$ linear growth rate in the $[C_\Omega, C_\alpha]$ plane. The thicker contours corresponds to $\sigma = 0$, and solid contours to $\sigma > 0$. All solutions are of antisymmetric parity and have $w/R = 0.1$, $\eta_e/\eta_c = 0.01$, and $\mathrm{R}_m = 0$. Solutions left of the thick-dashed line are steady ($\omega = 0$, α^2-like), and oscillatory to its right. Qualitatively similar diagrams are obtained for symmetric modes, other values of w/R, and/or solutions with positive C_α.

in symmetric solutions, and/or for positive-C_α solutions. Nonetheless, the transition from the α^2 to the $\alpha^2\Omega$ dynamo regime occurs smoothly as differential rotation is increased.

11.2.3 Getting the magnetic field to the surface

For our adopted value $\eta_c = 10^{13}\,\mathrm{cm}^2\,\mathrm{s}^{-1}$, $C_\Omega = 300$ amounts to $\Delta\Omega_0/\Omega_* \simeq 10^{-3}$, i.e., very weak differential rotation. Extant observations (and inferences) of magnetic fields in upper main-sequence stars currently have little to say about the steady/oscillatory character of the underlying field. Even if it were oscillating with a regular period of the order of a few years, as do the $\alpha^2\Omega$ solutions discussed here, it is not at all clear that the mechanism(s) responsible for bringing the field to the surface may not introduce additional temporal variabilities that would mask the underlying cycle period. If on the other hand the magnetic fields are shown to be strictly steady, one would then be forced to conclude that the same magnetic fields have obliterated any angular velocity difference between the core and envelope, something which they can in fact achieve quite efficiently in the absence of internal or external forcing.

The outstanding difficulty in explaining surface magnetism of massive stars by core dynamo action remains bringing the dynamo-generated magnetic field from the convective core to the surface, across the stably-stratified, low-diffusivity radiative envelope. For O and B main-sequence stars, estimates for the diffusion time yield values largely in excess of the main-sequence lifetime. Introducing thermally-driven meridional circulation in the radiative envelope, expected to be a significant internal flow in rapidly rotating stars, does accelerate the transport of the deep field to the surface, but also impedes dynamo action. Another possibility is that the dynamo-generated magnetic field manages to produce toroidal flux ropes that then rise

buoyantly to the surface. The analogy with the sun becomes even more compelling if a rotational shear layer does exist at the boundary between the inner convective core and outer radiative envelope. However, and unlike in the solar case, here the toroidal flux ropes are rising through a *stably* stratified environment, and so lose their buoyant force as they rise, because they cool faster as they rise than the surrounding stratification. Calculations performed in the thin flux tube stratification suggest that such toroidal flux ropes, assuming they do form, could rise perhaps halfway across the radiative envelope, but are unlikely to make it all the way to the surface through buoyancy alone. References listed in the bibliography should provide helpful entry points into the literature to those interested in further pursuing this aspect of massive star magnetism.

Problems:

They are your class projects! In fact I am counting on you all so that in the next version of these class notes, this final chapter will contains more illustrative material. Thanks in advance to all future contributors!

Bibliography:

The following is an early paper on the interpretation the Mt Wilson Ca emission dataset within the context of mean-field dynamo models, still well-worth reading:

Noyes, R.W., Weiss, N.O., & Vaughan, A.H., *Astrophys. J.*, **287**, 769 (1984)

In this context see also

Brandenburg, A., Saar, S.H., & Turpin, C.R., *Astrophys. J.*, **498**, L51 (1998).
Saar, S.H., & Brandenburg, A., *Astrophys. J.*, **524**, 295 (1999).

There has been renewed interest recently in the possibility that dynamo action could take place in the radiative envelope of massive stars, through turbulence asociated with a global instability of ther magnetic field itself. The possibility has been endorsed with enthusiasm by some stellar modellers, primarily because the said turbulence would also cause enhanced chemical mixing, known to be required to properly fit evolutionary tracks of massive stars, but whose origin remains mysterious. The operation of the associated dynamo remains nebulous, but those interested should take a look at

Spruit, H.C., *Astron. Astrophys.*, **381**, 923 (2002),
Braithwaite, J., *Astron. Astrophys.*, **449**, 451 (2006).

The linear α^2 and $\alpha^2\Omega$ models for core dynamo action in massive stars presented in §11.2 are taken pretty directly from

Charbonneau, P., & MacGregor, K.B. 2001, ApJ, 559, 1094.

This paper also adresses the effects of thermally-driven meridional circulation in the radiative envelope, including its deleterious effect on core dynanmo action. On $\alpha^2\Omega$ dynamo waves, see

Choudhuri, A.R., *Astrophys. J.*, **355**, 733 (1990),.
DeLuca, E.E., Gilman, P.A., *Geophys. Astrophys. Fluid Dyn.*, **43**, 119 (1988).

The difficulty in bringing the magnetic fields produced by core dynamo action to the surface of a star with a thick radiative envelope was cogently demonstrated a while ago by

Levy, E.H., & Rose, W.K. 1974, ApJ, 193, 419,
Schüssler, M., & Pähler, A. 1978, A&A, 68, 57.

For calculations of buoyantly rising thin flux tubes in the radiative envelope of massive stars, see

MacGregor, K.B., & Cassinelli, J., *Astrophys. J.*, **586**, 480 (2003).